Dynamics of field-driven domain-wall propagation in ferromagnetic nanowires

GEOFFREY S. D. BEACH*, CORNELIU NISTOR, CARL KNUTSON, MAXIM TSOI AND JAMES L. ERSKINE

Department of Physics, The University of Texas at Austin, Austin, Texas 78712-0264, USA

*e-mail: gbeach@physics.utexas.edu

Published online: 25 September 2005; doi:10.1038/nmat1477

Ferromagnetic nanowires are likely to play an important role in future spintronic devices. Magnetic domain walls, which separate regions of opposing magnetization in a nanowire, can be manipulated[1–6] and used to encode information for storage[2,7] or to perform logic operations[1]. Owing to their reduced size and dimensionality, the characterization of domain-wall motion is an important problem. To compete with other technologies, high-speed operation, and hence fast wall propagation, is essential. However, the domain-wall dynamics in nanowires has only been investigated[8–13] in the last five years and some results indicate a drastic slowing down of wall motion in higher magnetic fields[8]. Here we show that the velocity-field characteristic of a domain wall in a nanowire shows two linear regimes, with the wall mobility at high fields reduced tenfold from that at low fields. The transition is marked by a region of negative differential mobility and highly irregular wall motion. These results are in accord with theoretical predictions that, above a threshold field, uniform wall movement gives way to turbulent wall motion, leading to a substantial drop in wall mobility[13–19]. Our results help resolve contradictory reports of wall propagation velocities in laterally confined geometries[8,9], and underscore the importance of understanding and enhancing the breakdown field for practical applications.

A key dynamic parameter for magnetic domain-wall motion is the domain-wall mobility (μ) or the rate of change of wall velocity (v) with increasing external field (H). The mobility, and hence the limiting operating speed of devices based on domain-wall motion, is closely related to the intrinsic damping of spin precession. In the simplest theoretical model[17,18], the domain-wall velocity is given by $v = \mu H$ with the mobility $\mu = (\gamma\Delta/\alpha)$, where Δ and α are the domain-wall width and phenomenological Gilbert damping parameter, respectively, and γ is the gyromagnetic ratio. In permalloy ($Ni_{80}Fe_{20}$; or Py), a widely used soft magnetic alloy, $\Delta \sim 20$ nm and $\alpha \sim 0.01$, and domain-wall mobilities of $\sim$30–40 m s^{-1} Oe^{-1} are expected and observed in large-area thin Py films[20]. However, a very low μ of 2.6 m s^{-1} Oe^{-1} in a 500-nm-wide Py nanowire has been reported[8]. This low mobility was thought to arise from the enhanced relative contribution of edge roughness to the viscous damping of the domain-wall motion. A later study[9] found a mobility exceeding 30 m s^{-1} Oe^{-1} in a Py nanowire, despite its width being less than half the width of the wire in ref. 8. Because potential applications hinge upon the rate of domain-wall propagation, it is of great importance to rectify the conflicting experimental observations.

We present spatially resolved dynamic measurements of domain-wall propagation in a ferromagnetic nanowire over a broad field range. A Ta(3 nm)/Py(20 nm)/Ta(5 nm) trilayer was sputter-deposited and milled by a focused ion beam to form the 600 nm by 20 μm nanowire shown in the scanning electron micrograph (FEI Strata DB235) of Fig. 1c. One end of the wire was contiguous with the large-area film, providing a source for domain walls[5,6] nucleated at the relatively low coercive field of the latter. The other end was fashioned into a point to inhibit domain-wall nucleation within the nanowire[21]. The substrate, a 125-μm-thick silicon wafer, was held against a 500-μm-wide copper wire of semicircular cross-section. That wire was coupled inductively to a broadband radio-frequency power amplifier, providing a fast-risetime (<20 ns) bipolar magnetic field in excess of 70 Oe. The a.c. field magnitude was calibrated to better than 5% by measuring hysteresis loop shifts induced by an external d.c. bias field.

The longitudinal magneto-optical Kerr effect (MOKE) was used to detect spatially resolved magnetization reversal within the nanowire. A magnetic shape anisotropy field[22] of $\sim$500 Oe restricted the nanowire magnetization to lie along its axis, which was oriented in the optical plane defined by a continuous-wave laser incident at 45°. The laser was polarized normal to the optical plane and focused to an elliptical gaussian spot of 2.5 μm full width (at $1/e$ intensity along the long axis, measured using a knife-edge technique). Rotation of the polarization axis on reflection was proportional to the longitudinal component of magnetization and was used as a local probe of magnetization reversal. Nanosecond time resolution was achieved by using fast-risetime (<1 ns) photomultiplier tubes for detection, combined with high-bandwidth amplification and a 1-GHz-bandwidth oscilloscope.

Constant-field domain-wall propagation in the nanowire was studied using fast-risetime field steps. Measurements consisted of incrementing alternately the position of the probe laser spot along the nanowire and measuring the time-resolved MOKE at that position. Approximately 3×10^5 reversal cycles were averaged at each position to accumulate sufficient statistics; the consequences

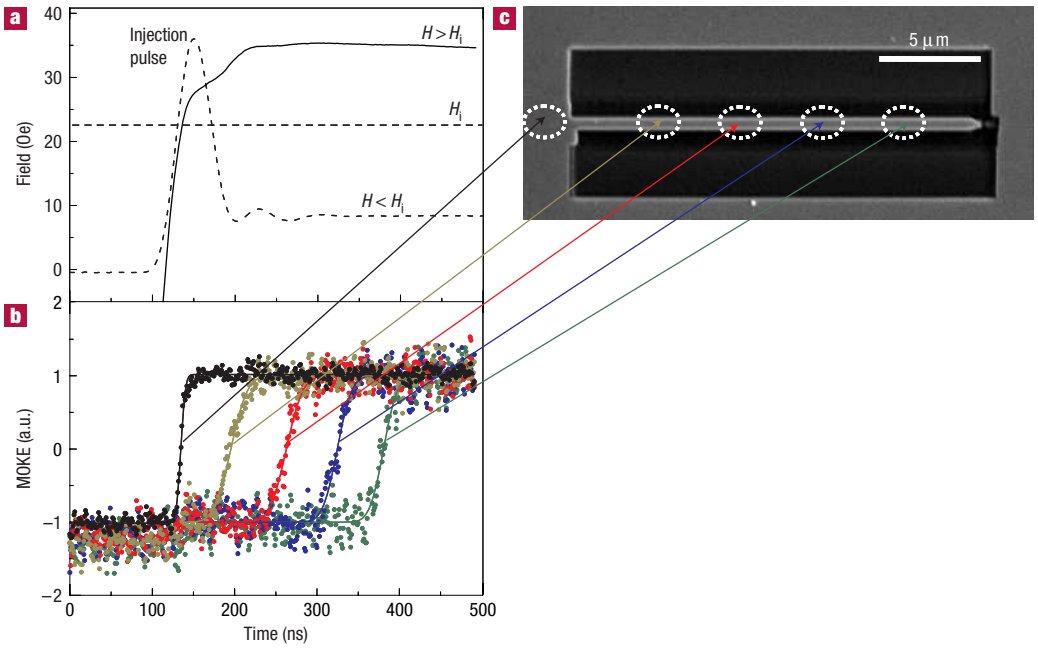

Figure 1 Field-driven magnetization reversal measurements. a, Example drive-field waveforms used for fields above (solid line) and below (dashed line) the wall injection field, H_i. Negative-going saturation pulses (not shown) preceded the positive-going field. **b**, Time-resolved MOKE signal (symbols) and fits to the error function (solid lines), in response to the 35 Oe field waveform of **a**. The MOKE transients were measured at the nanowire locations indicated in **c**. **c**, The scanning electron micrograph; ellipses approximate the measured $1/e$ width of the laser spot (incident at 45°).

of the repetitive nature of the measurements are addressed below. MOKE reversal transients measured after application of a field-step waveform (Fig. 1a) are shown in Fig. 1b for several positions. Reversal begins in the large-area film and proceeds along the nanowire with a progressive delay that increases linearly with distance from the film–nanowire junction. This behaviour implies domain-wall-mediated reversal, and the narrow temporal width of the (averaged) transients indicates that the process is highly repetitive from cycle to cycle.

Each reversal transient was fitted with an error function, representing the integrated intensity of the MOKE signal as a domain wall traverses the gaussian laser spot. The domain-wall arrival time (t_R) and reversal transient duration (τ_R) at each measurement location were taken as the centre and full-width (at $1/e$ intensity of the corresponding gaussian), respectively, of these fits. In Fig. 2a, t_R versus position is plotted for several field amplitudes. In all cases, the linear advance of the reversal boundary indicates constant average wall velocity. Any initial acceleration of the wall occurs rapidly on length and timescales below our resolution (and would be obscured by the finite risetime of the field step). The average wall velocities were taken from the inverse slope of t_R versus position, including only reversals that occurred after H was constant to within ~5%. These velocities are plotted versus H in Fig. 2b, with H ranging from 70 Oe down to the domain-wall 'injection field', $H_i = 24$ Oe, below which the nanowire magnetization does not reverse. In this region, the velocity increases linearly with H, with a mobility of 2.5(1) m s^{-1} Oe^{-1}. This value is much smaller than the mobilities typical of similar large-area films and is remarkably close to that reported in the 500-nm Py nanowire of ref. 8.

Step fields of amplitude below H_i, although able to reverse the large-area film, are insufficient to inject a domain wall into the nanowire. However, using specially tailored drive-field waveforms, we were able to extend our study of constant-field wall propagation far below H_i. An example field waveform is shown in Fig. 1a, and consists of a field step with $H < H_i$ preceded by a domain-wall 'injection pulse'. This injection pulse exceeds the injection field for a short duration, sufficient to inject a domain wall into the nanowire and propagate that wall ~5 μm along the wire. The pulse is followed by a constant non-zero field for wall-velocity evaluation. Fields down to ~1.5 Oe were sufficient to propagate an injected domain wall; below that field value, the averaged MOKE signal fell markedly, indicating that local pinning impeded wall propagation.

The reversal transients measured below H_i were similar to those shown in Fig. 1b, and indicated constant- (average-) velocity wall propagation after H had settled to a constant value. Viewed over this extended range, the v–H characteristic (Fig. 2b) becomes considerably more complex. At the lowest fields, the average velocity increases linearly with H at a rate of ~25 m s^{-1} Oe^{-1}. The velocity peaks at a critical field $H_p \approx 4.0$ Oe, above which it begins to decrease with increasing H. The negative differential mobility in this regime gradually increases and becomes positive again above ~20 Oe. For $H > 30$ Oe the v–H characteristic regains linearity, but with a tenfold reduction in μ from the low-H case.

Our results are largely in accord with the one-dimensional models of domain-wall motion developed in Walker[14] and generalized in refs 15,16. Although the authors of these articles considered a different anisotropy and field geometry, the key results remain applicable to the present case[12]. At low fields, Walker identified an exact stationary-state solution to the domain-wall equations of motion, giving the well-known linear mobility relation with $\mu = (\gamma\Delta/\alpha)$. This solution exists only up to a critical field H_W (the 'Walker field'), as the plane of transverse wall magnetization cants increasingly away from the direction of wall motion. Above H_W, the canting angle ϕ precesses continually, and the wall alternates between Néel (spins lying in the film plane) and Bloch (spins normal to the film plane). This precession, at a frequency[12] $\dot{\phi} = \gamma\sqrt{H^2 - H_W^2}$, leads to oscillatory wall motion because of the

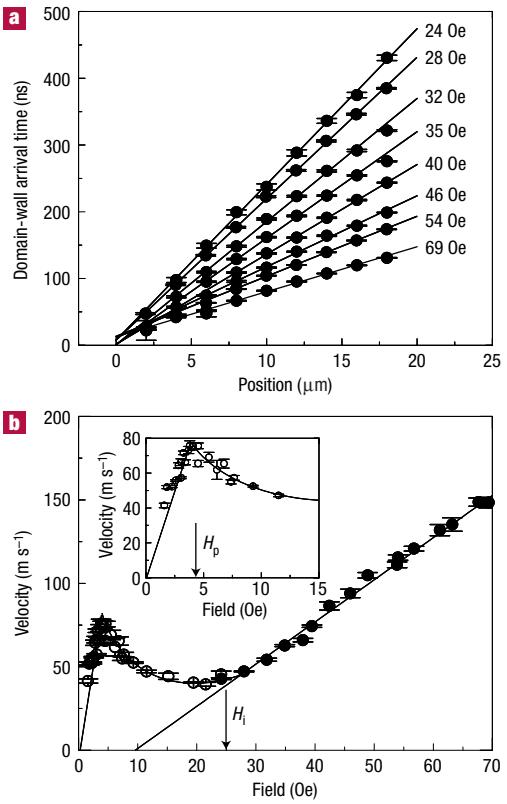

Figure 2 Domain-wall propagation and mobility characteristics. The error bars represent the standard deviations of the fitted quantities. **a**, Zero-crossing time of MOKE reversal transients as a function of position along the nanowire, with zero being the wire–film junction. Data for a range of field step amplitudes are shown. The solid lines are least-squares fits, whose slopes give the inverse average domain-wall velocity. **b**, Average domain-wall velocity versus field step amplitude. Arrows mark the domain-wall injection field, H_i, and velocity peak, H_p. Straight solid lines are linear fits to the data below H_p and above H_i, respectively; the curved line is a visual guide. Filled symbols show velocities obtained for a square-wave drive field and open symbols those obtained using injection pulse waveforms, such as in Fig. 1a, described in the text. The inset shows the detail around the velocity peak.

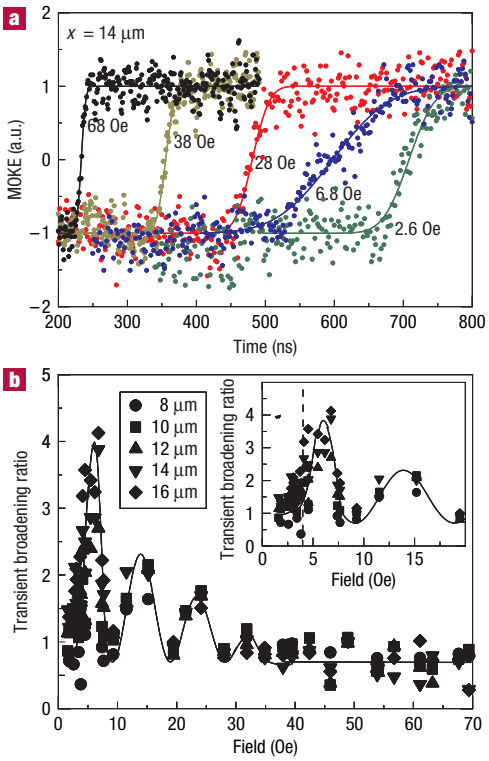

Figure 3 Reversal transient widths. a, Reversal transients measured 14 μm from the film–nanowire junction showing variation of width with field. Solid lines are fits to the error function. The transients for 6.8 and 2.6 Oe, just above and just below the critical field, respectively, have been shifted horizontally for clarity. **b**, Ratio of the measured reversal transient widths to those expected for a domain wall moving at velocity v_{avg} across a laser spot of width σ, where v_{avg} is the average velocity reported in Fig. 2b. Data are included for several measuring positions. Solid lines are visual guides. The dashed line in the inset marks the peak field from Fig. 2b.

periodic dependence of the field-torque terms on ϕ. For weak damping, the net average wall velocity begins decreasing with increasing H until, for $H \gg H_W$, the periodic torque terms tend to average out[17]. This leaves the damping torque, $\alpha\Delta\dot{\phi}$, as the sole contributor to net motion and results in an asymptotically linear v–H characteristic with a mobility $\mu = \gamma\Delta/(\alpha + \alpha^{-1})$. For low damping ($\alpha \ll 1$), the mobility at high fields is reduced significantly from its low-field value. These one-dimensional models thus account qualitatively for the data of Fig. 2b.

Our experiments also provide evidence for the predicted oscillatory wall motion above breakdown. During each reversal cycle, a domain wall traverses the probe laser spot of $(1/e)$ width σ in a time σ/v_{ins}, where v_{ins} is the instantaneous velocity at the observation point. For a uniformly propagating domain wall, the instantaneous and average velocities (v_{avg}) coincide, and τ_R should scale inversely with the average velocity shown in Fig. 2b. However, above breakdown, v_{ins} should vary with time and hence with position along the nanowire. If the length scale of the oscillatory motion exceeds σ, then the measured τ_R will deviate from σ/v_{avg}.

Figure 3a shows reversal transients at several fields measured at a distance $x = 14$ μm from the film–nanowire junction. In all cases, the transients are well described by an error function. At higher H, τ_R follows σ/v_{avg}. However, despite the nearly identical average wall velocities at $H = 38$ and 6.8 Oe, the transient for the latter is ~150 ns broader than that of the former. At $H < H_p$, the τ_R again approach σ/v_{avg}. Thus, the transient broadening at intermediate H is not due to the onset of domain-wall pinning because such pinning effects would increase with decreasing H. Rather, it indicates a transition to non-uniform wall motion above breakdown.

Because the measured reversal transients are averaged over many reversal cycles, two limiting cases must be considered when interpreting τ_R. In the 'jitter-free' case, the wall follows an identical trajectory from cycle to cycle and τ_R probes directly the (inverse) local instantaneous velocity. At a given $H > H_p$, τ_R should thus show periodic modulation with position along the nanowire owing to the oscillatory wall trajectory. Likewise, owing to the field dependence of the wall oscillation frequency given above, τ_R should vary periodically with H at a fixed position, as that position coincides alternately with velocity minima and maxima.

If instead the wall motion is non-repetitive from cycle to cycle, a random-phase description of the propagation is more appropriate. Here, oscillations in τ_R would be washed out by the averaging process. Instead, successive reversals would yield a distribution in wall arrival times (and instantaneous velocities) at each measurement position and a consequent broadening of τ_R from σ/v_{avg}. This broadening is a measure of the wall oscillation

amplitude about an average linear trajectory, which decreases as $1/H$ in the one-dimensional models.

Figure 3b compares the ratio of τ_R to σ/v_{avg} over the entire field range studied for several measurement positions. For a uniformly propagating wall, this ratio would be unity. In the jitter-free case, $\tau_R = \sigma/v_{ins}$ and the plotted quantity represents the ratio between the average and instantaneous velocities. In the random-phase limit, the ratio is proportional to the wall oscillation amplitude. Below H_p, τ_R approaches σ/v_{avg}, consistent with uniform wall motion below breakdown. As H exceeds H_p, the transient broadening ratio increases rapidly and varies periodically with H, approaching σ/v_{avg} at higher fields. The approximately $1/H$ dependence of the broadening ratio above H_p, expected in both the jitter-free and random-phase limits, indicates a transition to oscillatory wall motion with an amplitude that falls off with increasing H, as predicted above breakdown. The further periodic modulation with H is consistent with jitter-free oscillatory wall propagation. However, although periodic modulation of τ_R with position is then also expected, the data of Fig. 3b show no evidence of that periodicity, as the fields corresponding to maxima and minima in τ_R seem to be independent of position. The reason for the lack of a position dependence of τ_R is unclear. It would be expected in the random-phase limit, in which the transient broadening probes not the instantaneous velocity but rather its dispersion about the average velocity. However, in that case, the oscillations of τ_R with H are unexpected, as the broadening ratio should simply follow the $1/H$ dependence of the wall oscillation amplitude. Thus, although the data imply a transition from uniform wall propagation to irregular wall motion above H_p, these latter points remain to be understood.

We have observed and characterized a variety of behaviours in domain-wall transport in a laterally confined magnetic system. We find a linear v–H characteristic up to a peak field, followed by a region of negative differential mobility and irregular wall motion. At higher fields, v is again linear in H, but with a much lower average mobility. Our results are qualitatively consistent with one-dimensional models of domain-wall motion, which indicate a breakdown of smooth translational wall motion above a critical field. Negative differential mobility has seldom been observed because, for extended walls, it leads to wall instability[17]. A local backward perturbation in wall motion enhances the local effective drive due to surface tension that, for negative dv/dH, enhances that perturbation. However, in the one-dimensional limit, elastic wall deformations must vanish. The geometry in this experiment evidently approaches that limit.

The slope of v versus H over a limited field range, in a magnetic nanowire or any other system, is insufficient to draw conclusions about the intrinsic damping unless one knows the relation of that field range to the breakdown field. Thus, although the interpretations in refs 8,9 were contradictory, the data were not necessarily so. The velocity measurements for the Py nanowire in ref. 8, which found a mobility close to our high-field value, were made at significantly higher fields than those in ref. 9. The mobility of the latter study was comparable to our low-field result, indicating that those results may have been below the breakdown field. However, that would imply a breakdown field in that system much larger than the 4 Oe found here. Micromagnetic simulations[13] suggested that Walker breakdown in nanowires involves the nucleation and motion of Bloch lines (vortices) in the wall, and that finite roughness inhibits this process, pushing the breakdown field higher. In the thinner nanowire of ref. 9, this effect might become more prominent than in wider nanowires, pushing the breakdown field to a higher value. In light of this possibility, understanding and enhancing the breakdown field is critical for designing nanowires intended as rapid conduits for domain-wall propagation.

Received 27 May 2005; accepted 4 August 2005; published 25 September 2005.

References

1. Allwood, D. A. *et al.* Submicrometer ferromagnetic NOT gate and shift register. *Science* **296,** 2003–2006 (2002).
2. Tsoi, M., Fontana, R. E. & Parkin, S. S. P. Magnetic domain wall motion triggered by an electric current. *Appl. Phys. Lett.* **83,** 2617–2619 (2003).
3. Yamaguchi, A. *et al.* Real-space observation of current-driven domain wall motion in submicron magnetic wires. *Phys. Rev. Lett.* **92,** 077205 (2004).
4. Kläui, M. *et al.* Controlled and reproducible domain wall displacement by current pulses injected into ferromagnetic ring structures. *Phys. Rev. Lett.* **94,** 106601 (2005).
5. Shigeto, T., Shinjo, T. & Ono, T. Injection of a magnetic domain wall into a submicron magnetic wire. *Appl. Phys. Lett.* **75,** 2815–2817 (1999).
6. Cowburn, R. P., Allwood, D. A., Xiong, G. & Cooke, M. D. Domain wall injection and propagation in planar permalloy nanowires. *J. Appl. Phys.* **91,** 6949–6951 (2002).
7. Grollier, J. *et al.* Switching a spin valve back and forth by current-induced domain wall motion. *Appl. Phys. Lett.* **83,** 509–511 (2003).
8. Ono, T. *et al.* Propagation of a domain wall in a submicrometer magnetic wire. *Science* **284,** 468–470 (1999).
9. Atkinson, D. *et al.* Magnetic domain-wall dynamics in a submicrometre ferromagnetic structure. *Nature Mater.* **2,** 85–87 (2003).
10. Saitoh, E., Miyajima, H., Yamaoka, T. & Tatara, G. Current-induced resonance and mass determination of a single magnetic domain wall. *Nature* **432,** 203–206 (2004).
11. Nakatani, Y., Hayashi, N., Ono, T. & Miyajima, H. Computer simulation of domain wall motion in a magnetic strip line with submicron width. *IEEE Trans. Magn.* **37,** 2129–2131 (2001).
12. Thiaville, A., García, J. M. & Miltat, J. Domain wall dynamics in nanowires. *J. Magn. Magn. Mater.* **242–245,** 1061–1063 (2002).
13. Nakatani, Y., Thiaville, A. & Miltat, J. Faster magnetic walls in rough wires. *Nature Mater.* **2,** 521–523 (2003).
14. Schryer, N. L. & Walker, L. R. The motion of 180° domain walls in uniform dc magnetic fields. *J. Appl. Phys.* **45,** 5406–5420 (1974).
15. Slonczewski, J. C. Dynamics of magnetic domain walls. *Int. J. Magn.* **2,** 85–97 (1972).
16. Slonczewski, J. C. Theory of Bloch-line and Bloch-wall motion. *J. Appl. Phys.* **45,** 2705–2715 (1974).
17. Malozemoff, A. P. & Slonczewski, J. C. *Magnetic Domain Walls in Bubble Materials* (Academic, New York, 1979).
18. Hubert, A. & Schäfer, H. *Magnetic Domains* (Springer, Berlin, 1998).
19. Redjdal, M., Giusti, J., Ruane, F. F. & Humphrey, F. B. Thickness dependent wall mobility in thin permalloy films. *J. Appl. Phys.* **91,** 7547–7549 (2002).
20. Konishi, S., Yamada, S. & Kusuda, T. Domain-wall velocity, mobility, and mean-free-path in permalloy films. *IEEE Trans. Magn.* **7,** 722–724 (1971).
21. Kirk, K. J., Chapman, J. N. & Wilkinson, C. D. W. Switching fields and magnetostatic interactions of thin film magnetic nanoelements. *Appl. Phys. Lett.* **71,** 539–541 (1997).
22. Aharoni, A. Demagnetizing factors for rectangular ferromagnetic prisms. *J. Appl. Phys.* **83,** 3432–3434 (1998).

Acknowledgements

This work was supported by the NSF (NIRT program) under DMR-0404252 and by the R. A. Welch Foundation (F-1015). Instrumentation used in this work was developed and purchased through support from the NSF (IMR program) DMR-0216726 and from the Texas Coordinating Board (ATP-0099). Nanowires were fabricated using facilities of the Center for Nano and Molecular Science and Technology at UT Austin, supported in part by the R. A. Welch Foundation and by SPRING. Correspondence and requests for materials should be addressed to G.S.D.B.

Competing financial interests

The authors declare that they have no competing financial interests.